

LETTER TO THE EDITOR

Pure hydrocarbon cycles in TMC-1: Discovery of ethynyl cyclopropenylidene, cyclopentadiene and indene. [★]

J. Cernicharo¹, M. Agúndez¹, C. Cabezas¹, B. Tercero^{2,3}, N. Marcelino¹, J. R. Pardo¹, P. de Vicente²

¹ Grupo de Astrofísica Molecular, Instituto de Física Fundamental (IFF-CSIC), C/ Serrano 121, 28006 Madrid, Spain
e-mail: jose.cernicharo@csic.es

² Centro de Desarrollos Tecnológicos, Observatorio de Yebes (IGN), 19141 Yebes, Guadalajara, Spain

³ Observatorio Astronómico Nacional (OAN, IGN), Madrid, Spain

Received; accepted

ABSTRACT

We report the detection for the first time in space of three new pure hydrocarbon cycles in TMC-1: *c*-C₃HCCH (ethynyl cyclopropenylidene), *c*-C₅H₆ (cyclopentadiene) and *c*-C₉H₈ (indene). We derive a column density of $3.1 \times 10^{11} \text{ cm}^{-2}$ for the former cycle and similar values, in the range $(1-2) \times 10^{13} \text{ cm}^{-2}$, for the two latter molecules. This means that cyclopentadiene and indene, in spite of their large size, are exceptionally abundant, only a factor of five less abundant than the ubiquitous cyclic hydrocarbon *c*-C₃H₂. The high abundance found for these two hydrocarbon cycles, together with the high abundance previously found for the propargyl radical (CH₂CCH) and other hydrocarbons like vinyl and allenyl acetylene (Agúndez et al. 2021; Cernicharo et al. 2021a,b), start to allow us to quantify the abundant content of hydrocarbon rings in cold dark clouds and to identify the intermediate species that are probably behind the in situ bottom-up synthesis of aromatic cycles in these environments. While *c*-C₃HCCH is most likely formed through the reaction between the radical CCH and *c*-C₃H₂, the high observed abundances of cyclopentadiene and indene are difficult to explain through currently proposed chemical mechanisms. Further studies are needed to identify how are five- and six-membered rings formed under the cold conditions of clouds like TMC-1.

Key words. molecular data – line: identification – ISM: molecules – ISM: individual (TMC-1) – astrochemistry

1. Introduction

Since the hypothesis that polycyclic aromatic hydrocarbons (PAHs) are the carriers of the unidentified infrared bands (Léger & Puget 1984; Allamandola et al. 1985), many efforts have been devoted to understand the chemical processes leading to the formation of these molecular species (see, e.g., Joblin & Cernicharo 2018). Circumstellar envelopes around carbon-rich Asymptotic Giant Branch (AGB) stars have been suggested as the factories of PAHs (Cherchneff et al. 1992). The detection of benzene in the carbon-rich protoplanetary nebula CRL 618 (Cernicharo et al. 2001) suggests a bottom-up approach in which the small hydrocarbons formed during the AGB phase, such as C₂H₂ and C₂H₄, interact with the ultraviolet (UV) radiation produced by the star in its evolution to the white dwarf phase (Woods et al. 2002; Cernicharo 2004). Other hypotheses involve the processing of dust grains around evolved stars, either through UV photons (Pillari et al. 2015) or by chemical processes (Martínez et al. 2020). Hence, it has been surprising to see that cyanide derivatives of PAHs have been found in a cold prestellar core such as TMC-1, which is well protected against UV radiation (McGuire et al. 2018, 2021). It is unlikely that these PAH-cyanides arise from a reservoir of PAHs existing since the early stages of the cloud,

[★] Based on observations carried out with the Yebes 40m telescope (projects 19A003, 20A014, 20D023, and 21A011) and the Institut de Radioastronomie Millimétrique (IRAM) 30m telescope. The 40m radiotelescope at Yebes Observatory is operated by the Spanish Geographic Institute (IGN, Ministerio de Transportes, Movilidad y Agenda Urbana). IRAM is supported by INSU/CNRS (France), MPG (Germany) and IGN (Spain).

since these relatively small PAHs would not have survived the diffuse cloud stage. Although McGuire et al. (2021) propose a reasonable chemical network starting with the phenyl radical that could explain the observed abundances of cyanonaphthalene, the chemical routes leading to benzene itself are still unclear. An in situ formation mechanism for benzene must involve abundant hydrocarbons containing from 2 to 4 carbon atoms. Moreover, some of these species have to permit an easy cyclization in 2-3 steps to have an efficient yield of benzene or phenyl radical. The propargyl radical, CH₂CCH, has been found recently in TMC-1 by Agúndez et al. (2021) with an abundance close to 10⁻⁸ relative to H₂. In addition, complex hydrocarbons such as vinyl and allenyl acetylene have been also observed with very large abundances (Cernicharo et al. 2021a,b). These hydrocarbons may hold the key to form the first aromatic ring, from which larger PAHs can grow.

In this Letter we report the discovery of three pure hydrocarbon cycles (see Fig. 1): *c*-C₃HCCH (ethynyl cyclopropenylidene), *c*-C₅H₆ (cyclopentadiene), and *c*-C₉H₈ (indene)¹.

2. Observations

New receivers, built within the Nanocosmos project², and installed at the Yebes 40m radiotelescope, were used for the obser-

¹ We have learned in a virtual seminar during the final phase of preparation of this work that a paper has been submitted (Burkhardt et al., 2021) claiming the detection of this species in TMC-1. We do not know neither its content nor the quality of the detection.

² <https://nanocosmos.iff.csic.es/>

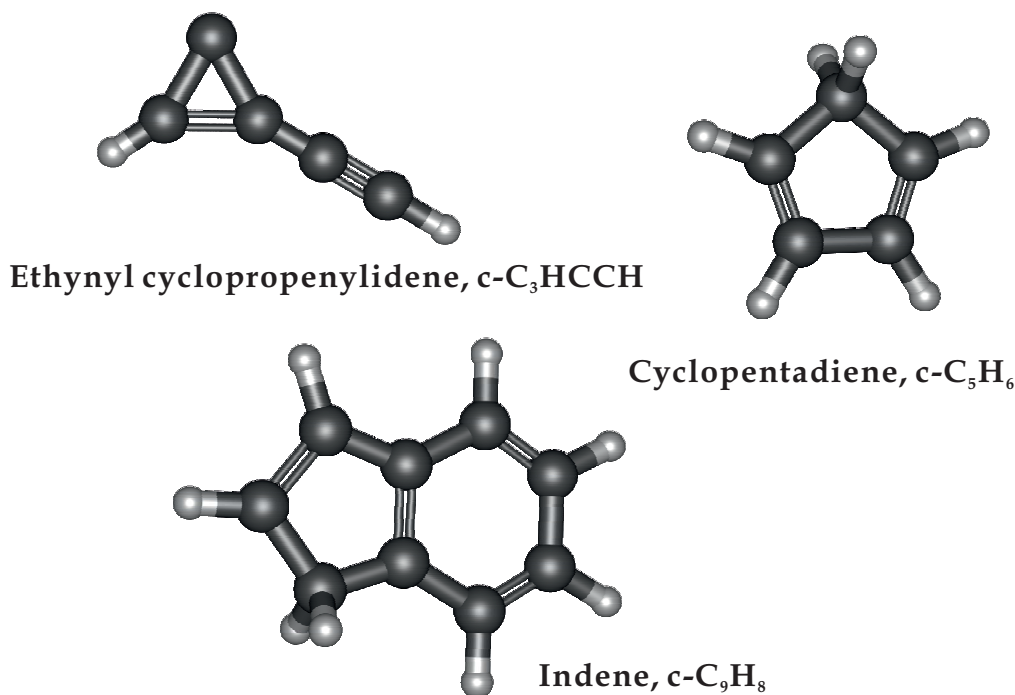


Fig. 1. Structures of the three species detected in this work.

vations of TMC-1. The Q-band receiver consists of two HEMT cold amplifiers covering the 31.0-50.3 GHz band with horizontal and vertical polarizations. Receiver temperatures vary from 22 K at 32 GHz to 42 K at 50 GHz. The backends are $2 \times 8 \times 2.5$ GHz fast Fourier transform spectrometers with a spectral resolution of 38.15 kHz providing the whole coverage of the Q-band in both polarisations. The main beam efficiency varies from 0.6 at 32 GHz to 0.43 at 50 GHz. A detailed description of the system is given by Tercero et al. (2021).

The line survey of TMC-1 ($\alpha_{J2000} = 4^{\text{h}}41^{\text{m}}41.9^{\text{s}}$ and $\delta_{J2000} = +25^{\circ}41'27.0''$) in the Q-band was performed in several sessions. Previous results on the detection of C_3N^- and C_5N^- (Cernicharo et al. 2020b), HC_5NH^+ (Marcelino et al. 2020), HC_4NC (Cernicharo et al. 2020c), and HC_3O^+ (Cernicharo et al. 2020a) were based on two observing runs performed in November 2019 and February 2020. Two different frequency coverages were used, 31.08-49.52 GHz and 31.98-50.42 GHz, in order to check that no spurious spectral ghosts are produced in the down-conversion chain. Additional data were taken in October, December 2020 and January-April 2021. The observing procedure was frequency-switching with a frequency throw of 10 MHz for the two first runs and of 8 MHz for all the others.

All data were analyzed using the GILDAS package³.

3. Results

The sensitivity of our TMC-1 data is better than previously published line surveys of this source at the same frequencies (Kaifu et al. 2004) by a factor 10-20. In fact, it has been possible to detect many individual lines from molecules that were reported previously only by stacking techniques (Marcelino et al. 2021). The recent discovery of some molecules containing the ethynyl group (CCH), such as vinyl and allenyl acetylene (Cernicharo et al. 2021a,b), and of the propargyl radical (Agúndez et al. 2021),

prompted us to search for other chemically related hydrocarbons. Line identification in this work was done using the catalogues MADEX (Cernicharo 2012), CDMS (Müller et al. 2005), and JPL (Pickett et al. 1998).

3.1. Ethynyl cyclopropenylidene, $c\text{-C}_3\text{HCCH}$

Cyclopropenylidene ($c\text{-C}_3\text{H}_2$) is an abundant species in cold dark clouds. Several lines of the para species of this molecule have been detected in our line survey. They are analyzed in Appendix D. The reaction of this molecule with CCH and CN could lead to the formation of $c\text{-C}_3\text{HCCH}$ and $c\text{-C}_3\text{HCN}$. Ethynyl cyclopropenylidene ($c\text{-C}_3\text{HCCH}$; see Fig. 1) is one of the various C_5H_2 isomers (see Appendix B) studied by microwave spectroscopy in the laboratory (Travers et al. 1997; McCarthy et al. 1997; Gottlieb et al. 1998). In addition to $c\text{-C}_3\text{HCCH}$, these isomers are $l\text{-H}_2\text{C}_5$, the bent $\text{HCC}(\text{CH})\text{CC}$, and the cycle $c\text{-H}_2\text{C}_3\text{CC}$. All these species are implemented in the MADEX code (Cernicharo 2012). In the case of $c\text{-C}_3\text{HCCH}$, the dipole moment components are $\mu_a = 2.04$ D, and $\mu_b = 2.89$ D (Travers et al. 1997).

A search for $c\text{-C}_3\text{HCCH}$ resulted in the detection of 13 rotational lines, which gives a high degree of confidence in the detection of this species. Nevertheless, the lines are weak, with intensities around 1 mK. Some of them are shown in Fig. 2. The derived line parameters (see Appendix A) are given in Table A.1. A few lines that could have been detected in our survey appear blended with lines from other species or are affected by negative features produced in the folding of frequency switching procedure. These cases are indicated in Table A.1. An analysis of the observed intensities through a rotational diagram provides a rotational temperature of 8 ± 3 K and a column density for $c\text{-C}_3\text{HCCH}$ of $(3.1 \pm 0.8) \times 10^{11} \text{ cm}^{-2}$. We assumed a linewidth of 1.0 km s^{-1} , which corresponds to the observed average value, and a source of uniform brightness temperature with a diameter of $80''$ (Fossé et al. 2001). We performed a model fitting di-

³ <http://www.iram.fr/IRAMFR/GILDAS>

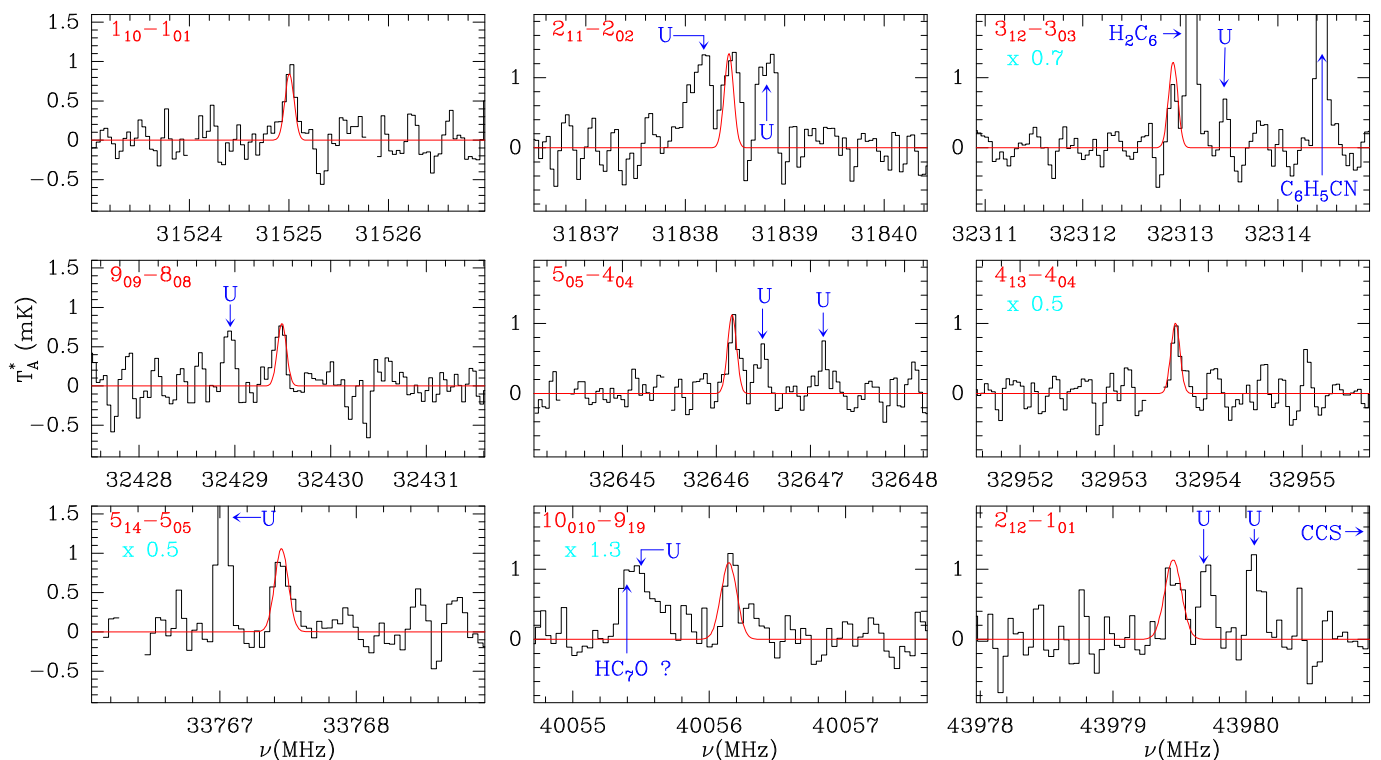


Fig. 2. Selected transitions of c -C₃HCCH in TMC-1. The abscissa corresponds to the rest frequency of the lines assuming a local standard of rest velocity of the source of 5.83 km s⁻¹. Frequencies and intensities for the observed lines are given in Table A.1. The ordinate is the antenna temperature, corrected for atmospheric and telescope losses, in milli Kelvin. The quantum numbers for each transition are indicated in the upper left corner of the corresponding panel. The red lines show the computed synthetic spectrum for this species for $T_r=10$ K and a column density of 3.1×10^{11} cm⁻². Cyan labels indicated the multiplicative factor applied to the model to match the intensity of the observed lines.

rectly the observed line profiles as described by Cernicharo et al. (2021c), with the result that the best match between the computed synthetic spectrum and the observations corresponds to $T_r = 10$ K and a column density similar to that derived from the rotation diagram. Figure 2 shows, in red, the computed synthetic spectrum. The correction factors applied to each line to match the observations are indicated in the Figure. Taken into account the signal-to-noise ratio of the data, these factors are within the expected uncertainties of the fit.

Adopting a column density of H₂ of 10^{22} cm⁻² for TMC-1 (Cernicharo & Guélin 1987), the abundance of c -C₃HCCH relative to H₂ is 3.1×10^{-11} , which is significantly below those of c -C₃H₂ and c -C₃H (5.9×10^{-9} and 6.2×10^{-10} , respectively; see Appendices D and E), ethynyl derivatives such as vinyl, methyl, and allenyl acetylene (Cernicharo et al. 2021a,b; Cabezas et al. 2021), and propylene (Marcelino et al. 2007). We derive the following abundance ratios: c -C₃H₂/ c -C₃HCCH ~ 190 (see Appendix D), c -C₃H/ c -C₃HCCH ~ 20 , and c -C₃H₂/ c -C₃H ~ 10 . Upper limits to the column densities of the isomers of c -C₃HCCH are analyzed in Appendix B. Improved rotational and distortion constants for c -C₃HCCH are given in Appendix C.

3.2. Cyclopentadiene, c -C₅H₆

The recent detection by stacking techniques of two cyanide derivatives of cyclopentadiene in TMC-1 (Lee et al. 2021) makes very likely that cyclopentadiene itself is also present in this source. Cyclopentadiene (see Fig. 1) has been observed in the laboratory up to 386.6 GHz by different authors (Laurie 1956; Scharpen & Laurie 1965; Benson & Flygare 1970; Bogey et al. 1988). The molecule has a low dipole moment of 0.416 D along

its b axis (Laurie 1956). Because of the C_{2v} symmetry of the molecule, two spin species, ortho and para, with $K_a + K_c$ odd and even, and statistical weights 9 and 7, respectively, have to be considered. The lowest ortho level is the 1_{1,1} and it is 0.6 K above the lowest para level (0_{0,0}). We searched for this species in our TMC-1 data and we detected all the strong lines in the 31-50 GHz frequency range. They are shown in Fig. 3 and the line parameters are given in Table A.1. Only one para line, the 4_{1,3} – 3_{2,2}, which is affected by a negative frequency-switching artifact, is missing. Another para line, the 4_{0,4} – 3_{1,3} is strongly blended with a line from c -C₃HD (see third panel from the top in Fig. 3). Taking into account the large geometrical section of the molecule and the low dipole moment, we could expect to have its rotational levels thermalized at the kinetic temperature of the cloud, 10 K. Assuming the same source parameters than for c -C₃HCCH we derive a total column density for cyclopentadiene of $(1.2 \pm 0.3) \times 10^{13}$ cm⁻², with identical contributions from the ortho and para species. The fractional abundance of c -C₅H₆ relative to H₂ is thus 1.2×10^{-9} . This abundance is identical to that of CH₂CHCCH (Cernicharo et al. 2021b) and H₂CCHCCH (Cernicharo et al. 2021c), and lower than that of the propargyl radical by a factor of ~ 7 (Agúndez et al. 2021). Compared with its cyano-derivatives (Lee et al. 2021), cyclopentadiene is 15 and 63 times more abundant than 1- and 2-cyanocyclopentadiene, respectively.

3.3. Indene, c -C₉H₈

Indene, c -C₉H₈, has a bicyclic structure with a six-membered ring fused to a five-membered ring (see Fig. 1). It has been studied in the microwave laboratory by Li et al. (1979) and Cami-

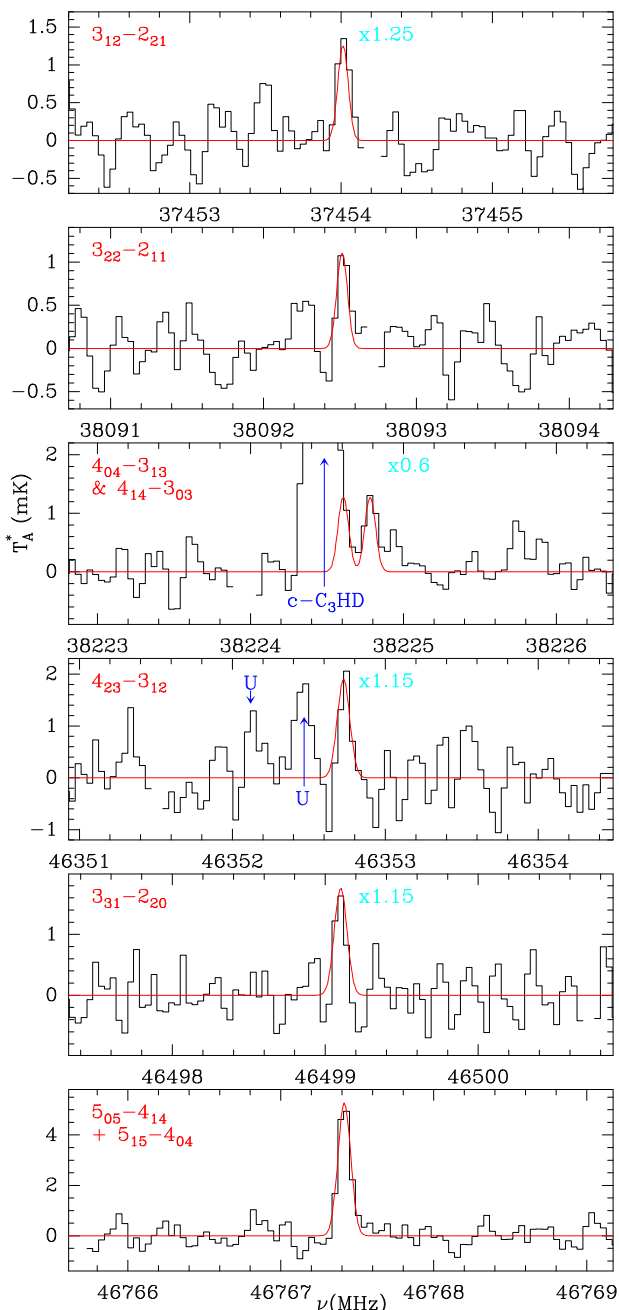


Fig. 3. Same as Fig. 2 but for the observed transitions of $c\text{-C}_5\text{H}_6$ towards TMC-1. The red line shows the computed synthetic spectrum for cyclopentadiene assuming $T_r = 10$ K and $N(c\text{-C}_5\text{H}_6) = 1.2 \times 10^{13} \text{ cm}^{-2}$. Cyan labels, when present, indicate the multiplicative factor applied to the best fit model to match the observations.

nati (1993). The accuracy of these measurements is moderate, with typical uncertainties for the measured frequencies of ~ 100 kHz. Its dipole moment is also relatively low, with $\mu_a = 0.50$ D and $\mu_b = 0.37$ D (Caminati 1993). Frequency predictions in the 31–50 GHz range have uncertainties between 10 and 80 kHz. We searched for indene in our data and found a large number of lines above the 3σ level. Nineteen of them are shown in Fig. 4. Line parameters for all the 47 observed lines of indene detected in TMC-1 are given in Table A.1. Improved rotational and distortion constants for indene are provided in Appendix C and Table C.2.

In order to derive a column density for indene we have assumed that the rotational temperature is 10 K. Taking into account the large geometrical section of the molecule and its low dipole moment, this assumption seems reasonable. The model fit procedure, consisting in a fit to the observed line profiles, provides a column density for indene of $(1.6 \pm 0.3) \times 10^{13} \text{ cm}^{-2}$, which is very similar to that of cyclopentadiene, vinyl and allenyl acetylene, and only a factor of five below that of $c\text{-C}_3\text{H}_2$. The fractional abundance of indene relative to H_2 is thus 1.6×10^{-9} . The discovery of this large hydrocarbon through the old fashion line-by-line detection procedure is solid and robust. For this species, the observed averaged value of the linewidth is close to 1.0 km s^{-1} , such as for $c\text{-CH}_3\text{CCH}$. Most lines of polar species have linewidths of 0.6 km s^{-1} . In the case of indene, its low dipole moment and its easy to be thermalized conditions, could favour the emission from the less dense regions of the cloud. This could suggest that this species prevails in the molecular envelope of TMC-1. However, $c\text{-CH}_3\text{CCH}$ has a larger dipole moment and requires a high density to be close to thermalization as derived in section 3.1. Further observations with higher spectral resolution are needed to discriminate between excitation and possible contribution from different cloud components.

4. Discussion

4.1. $c\text{-C}_3\text{HCCH}$

The most obvious route to $c\text{-C}_3\text{HCCH}$ is the reaction between CCH and $c\text{-C}_3\text{H}_2$. To our knowledge, this reaction has not been studied either experimentally or theoretically, but it is likely that it occurs fast at low temperatures with the H loss channel being the major one, based on the reactivity of CCH with other unsaturated hydrocarbons (Vakhtin et al. 2001). In addition, the two reactants are quite abundant in TMC-1 (e.g., Agúndez & Wakelam 2013). If we implement this reaction with a rate coefficient of $10^{-10} \text{ cm}^3 \text{ s}^{-1}$ in a chemical model similar to that presented by Agúndez et al. (2021) and we assume that $c\text{-C}_3\text{HCCH}$ is mostly destroyed by reactions with C atoms and C^+ and H^+ ions, the peak abundance calculated for $c\text{-C}_3\text{HCCH}$ is $\sim 5 \times 10^{-11}$ relative to H_2 , which is in very good agreement with the value observed in TMC-1. Although the subset of reactions involving $c\text{-C}_3\text{HCCH}$ is clearly incomplete, this exercise shows that the reaction $\text{CCH} + c\text{-C}_3\text{H}_2$ could be a plausible formation route for this cyclic hydrocarbon in TMC-1. Other reactions that could also yield $c\text{-C}_3\text{HCCH}$ are $c\text{-C}_3\text{H} + \text{C}_2\text{H}_2$ and $\text{C}_2 + \text{CH}_2\text{CCH}$, although little is known on their chemical kinetics.

Similarly to CCH, the radical CN has been also found to react rapidly with unsaturated hydrocarbons at low temperatures (e.g., Sims et al. 1993). Therefore, the reaction between CN and $c\text{-C}_3\text{H}_2$ is a very likely source of $c\text{-C}_3\text{HCN}$, which is the cyanide derivative analogue of $c\text{-C}_3\text{HCCH}$. It is interesting to note that ethynyl derivatives are more abundant than cyanide derivatives in TMC-1, e.g., $\text{CH}_3\text{CCCCH}/\text{CH}_3\text{CCCN} = 7.6$ and $\text{CH}_2\text{CCHCCH}/\text{CH}_2\text{CCHCN} = 4.4$ (Marcelino et al. 2021; Cernicharo et al. 2021b), which is thought to reflect the CCH/CN abundance ratio of 10 observed in this source (Pratap et al. 1997). Therefore, we could expect $c\text{-C}_3\text{HCN}$ to be a few times less abundant than $c\text{-C}_3\text{HCCH}$. We do not detect $c\text{-C}_3\text{HCN}$ in our sensitive TMC-1 data, which means that it must have a column density below $2.5 \times 10^{11} \text{ cm}^{-2}$ (3σ upper limit; see Appendix B). Therefore, the abundance ratio $c\text{-C}_3\text{HCCH}/c\text{-C}_3\text{HCN}$ in TMC-1 must be > 1.2 . It is therefore likely that a reduced noise level from deeper observations may lead to the detection of $c\text{-C}_3\text{HCN}$ in TMC-1.

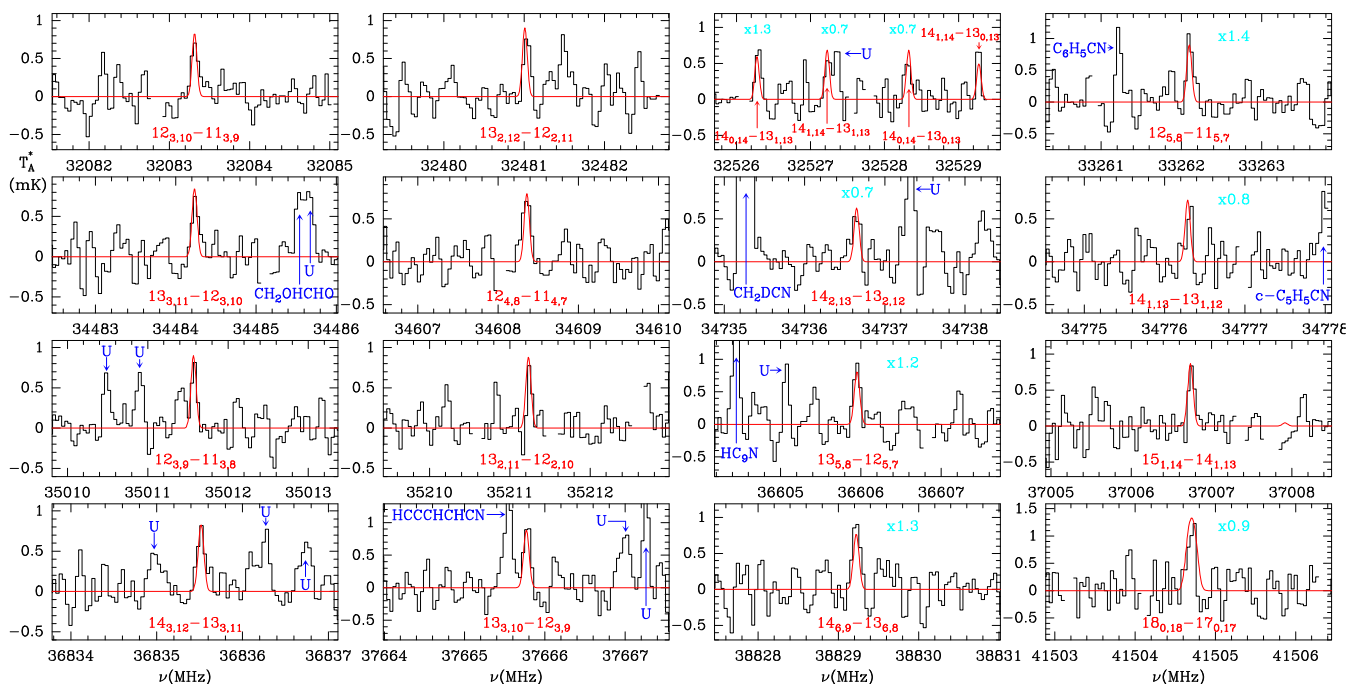


Fig. 4. Same as Fig. 2 but for the selected transitions of $c\text{-C}_9\text{H}_8$ observed towards TMC-1. The red line shows the computed synthetic spectrum for indene assuming $T_c = 10$ K and $N(c\text{-C}_9\text{H}_8) = 1.6 \times 10^{13} \text{ cm}^{-2}$. Cyan labels, when present, indicate the multiplicative factor applied to the best fit model to match the observations.

4.2. Cyclopentadiene, $c\text{-C}_5\text{H}_6$

Given the high abundance derived for cyclopentadiene in TMC-1, 1.2×10^{-9} relative to H_2 , it is not straightforward to find an efficient formation route. Several reactions that could lead to $c\text{-C}_5\text{H}_6$ are not efficient under the cold conditions of TMC-1. For example, the reaction between $\text{CH}_2\text{CCH} + \text{C}_2\text{H}_4$ has an activation barrier (Saeyns et al. 2003), while the reactions of C_2H_3 with either CH_3CCH or CH_2CCH_2 probably have also barriers, as occurs in other reactions of C_2H_3 with unsaturated hydrocarbons (Miller et al. 2000; Ismail et al. 2007; Goldsmith et al. 2009). The reaction between C_3H_5 and C_2H_2 yields cyclopentadiene, but it has a barrier (Bouwman et al. 2015). The reaction $\text{C}_2\text{H} + \text{CH}_2\text{CHCH}_3$ is fast at low temperatures and produces several C_5H_6 isomers, although the experimental data seems to be inconsistent with cyclopentadiene being one of them (Bouwman et al. 2012).

The reaction between CH and butadiene ($\text{CH}_2\text{CHCHCH}_2$) is calculated to produce $c\text{-C}_5\text{H}_6$ with no barrier (McCarthy et al. 2021). Adopting a rate coefficient of $10^{-10} \text{ cm}^3 \text{ s}^{-1}$ for this reaction in our chemical model, based on Agúndez et al. (2021), and assuming that $c\text{-C}_5\text{H}_6$ is mostly removed through reactions with C atoms and C^+ and H^+ ions, we calculate a peak abundance of $\sim 3 \times 10^{-13}$ relative to H_2 for $c\text{-C}_5\text{H}_6$. This is more than three orders of magnitude below the observed value. In the chemical model, butadiene is essentially formed by the reaction $\text{CH} + \text{CH}_2\text{CHCH}_3$ (Daugey et al. 2005; Loison & Bergeat 2009; Ribeiro & Mebel 2016) with a peak abundance of $\sim 3 \times 10^{-10}$ relative to H_2 . Butadiene is an interesting potential precursor of $c\text{-C}_5\text{H}_6$, and also of benzene (Jones et al. 2011), but to play such a role it needs to have an abundance much higher than calculated by current gas-phase chemical models. Unfortunately, it is a non-polar molecule and thus it cannot be detected through radio techniques.

Given the high abundance derived for the radical CH_2CCH (Agúndez et al. 2021), reactions between radicals, such as

$\text{CH}_2\text{CCH} + \text{C}_2\text{H}_5$ and $\text{C}_2\text{H}_3 + \text{CH}_2\text{CHCH}_2$, are also potential sources of $c\text{-C}_5\text{H}_6$. Routes involving ions, such as condensation reactions between cationic and neutral hydrocarbons (Herbst & Leung 1989), may also lead to $c\text{-C}_5\text{H}_6$. Theoretical studies on these reactions would help to evaluate their role in the synthesis of cyclopentadiene. Whatever the formation route to $c\text{-C}_5\text{H}_6$ is, this hydrocarbon cycle is the most obvious precursor of the two cyanide derivatives $c\text{-C}_5\text{H}_5\text{CN}$ detected in TMC-1 (McCarthy et al. 2021; Lee et al. 2021).

4.3. Indene, $c\text{-C}_9\text{H}_8$

The high abundance derived for this aromatic molecule, in fact the first pure polycyclic aromatic hydrocarbon found in space, also challenges to find out an efficient formation route in TMC-1. Such a route should involve a fast reaction between two abundant species. Potential formation reactions like $c\text{-C}_6\text{H}_6 + \text{CH}_2\text{CCH}$ and $c\text{-C}_6\text{H}_5 + \text{C}_3\text{H}_4$ have activation barriers (Kislov & Mebel 2007; Vereecken & Peeters 2003; Mebel et al. 2017). Reactions such as $c\text{-C}_5\text{H}_6 + \text{C}_4\text{H}_3$ or $c\text{-C}_5\text{H}_5 + \text{C}_4\text{H}_4$ could be efficient producing indene. Doddipatla et al. (2021) suggest that indene can be formed through the barrierless reaction between the radical CH and styrene ($c\text{-C}_6\text{H}_5\text{C}_2\text{H}_3$). However, it is unknown whether the precursor styrene is abundant enough in TMC-1, and it is not obvious which formation pathway can lead to it. Doddipatla et al. (2021) present a tentative synthetic route, from which they calculate abundances of up to 10^{-12} for indene, well below the value derived from observations here. It is clear that further research is needed to explain the presence of indene in TMC-1 with an abundance as high as 1.6×10^{-9} relative to H_2 .

5. Conclusions

We report the detection of $c\text{-C}_3\text{HCCH}$, cyclopentadiene, and indene in TMC-1. While the observed abundance of $c\text{-C}_3\text{HCCH}$, a few 10^{-11} relative to H_2 , can be accounted for by the reaction

between CCH and $c\text{-C}_3\text{H}_2$, the fairly high abundances found for cyclopentadiene and indene, above 10^{-9} , are difficult to explain by currently proposed formation routes. The detection of very abundant cyclopentadiene and indene should promote further research to elucidate which plausible bottom-up mechanisms of formation of such complex aromatic hydrocarbons can be at work in cold dense clouds like TMC-1.

Acknowledgements. We thank ERC for funding through grant ERC-2013-Syg-610256-NANOCOSMOS. We also thank Ministerio de Ciencia e Innovación of Spain (MICIU) for funding support through projects AYA2016-75066-C2-1-P, PID2019-106110GB-I00, PID2019-107115GB-C21 / AEI / 10.13039/501100011033, and PID2019-106235GB-I00. M.A. thanks MICIU for grant RyC-2014-16277. We would like to thank our referee, S. Yamamoto, for his useful comments and suggestions.

References

- Agúndez, M. & Wakelam, V. 2013, *Chem. Rev.* 113, 8710
- Agúndez, M., Cabezas, C., Tercero, B., et al. 2021, *A&A*, 647, L10
- Allamandola, L.J., Tielens, A.G.G.M. & Barker, J.R., 1985, *ApJ*, 290, L25
- Avery, L.W. & Green, S. 1989, *ApJ*, 337, 306
- Benson, R.C. & Flygare, W.H. 1970, *J. Am. Chem. Soc.*, 92, 7223
- Bogey, M., Demuyne, C., Destombes, J.L. 1988, *J. Mol. Spectrosc.*, 132, 277
- Bouwman, J., Goulay, F., Leone, S. R., & Wilson, K. R. 2012, *J. Phys. Chem. A*, 116, 3907
- Bouwman, J., Bodi, A., Oomens, J., & Hemberger, P. 2015, *PCCP*, 17, 20508
- Cabezas, C., Endo, Y., Roueff, E., et al. 2021, *A&A*, 646, L1
- Caminati, W. 1993, *J. Chem. Soc. Faraday Trans.*, 89, 4153 IRAM report (Granada: IRAM)
- Cernicharo, J. & Guélin, M. 1987, *A&A*, 176, 299
- Cernicharo, J., Guélin, M., Kahane, C. 2000, *A&ASuppl. Ser.*, 142, 181
- Cernicharo, J., Heras, A.M., Tielens, A.G.G.M., et al. 2001, *ApJ*, 546, L123
- Cernicharo, J. 2004, *ApJ*, 608, L41
- Cernicharo, J., 2012, in *ECLA 2011: Proc. of the European Conference on Laboratory Astrophysics*, EAS Publications Series, 2012, Ed.: C. Stehl, C. Joblin, & L. d'Hendecourt (Cambridge: Cambridge Univ. Press), 251; https://nanocosmos.iff.csic.es/?page_id=1619
- Cernicharo, J., Guélin, M., Agúndez, M., et al. 2018, *A&A*, 618, A4
- Cernicharo, J., Marcelino, N., Agúndez, M., et al. 2020a, *A&A*, 642, L17
- Cernicharo, J., Marcelino, N., Pardo, J.R., et al. 2020b, *A&A*, 641, L9
- Cernicharo, J., Marcelino, N., Agúndez, et al. 2020c, *A&A*, 642, L8
- Cernicharo, J., Agúndez, M., Cabezas, C., et al. 2021a, *A&A*, 647, L2
- Cernicharo, J., Agúndez, M., Cabezas, C., et al. 2021b, *A&A*, 647, L3
- Cernicharo, J., Cabezas, C., Endo, Y., et al. 2021c, *A&A*, 646, L3
- Cherchneff, I., Barker, J. R., & Tielens, A. G. G. M. 1992, *ApJ*, 401, 269
- Daugey, N., Caubet, P., Retail, B., et al. 2005, *PCCP*, 7, 2921
- Doddipatla, S., Galimova, G. R., Wei, H., et al. 2021, *Sci. Adv.*, 7, eabd4044
- Fossé, D., Cernicharo, J., Gerin, M., Cox, P. 2001, *ApJ*, 552, 168
- Goldsmith, C. F., Ismail, H., Abel, P. R., & Green, W. H. 2009, *Proc. Combust. Inst.*, 32, 139
- Gottlieb, C.A., McCarthy, M.C., Gordon, V.D., et al. 1998, *ApJ*, 509, L141
- Herbst, E. & Leung, C.M. 1989, *ApJS*, 69, 271
- Ismail, H., Goldsmith, C. F., Abel, P. R., et al. 2007, *J. Phys. Chem. A*, 111, 6843
- Joblin, C. & Cernicharo, J. 2018, *Science*, 359, 156
- Jones, B. M., Zhang, F., Kaiser, R. I., et al. 2011, *PNAS*, 108, 452
- Kaifu, N., Ohishi, M., Kawaguchi, K., et al. 2004, *PASJ*, 56, 69
- Khalifa, M.B., Sahnoun, E., Wiesenfeld, L. et al. 2019, *PCCP*, 21, 1443
- Kislov, V. V. & Mebel, A. M. 2007, *J. Phys. Chem. A*, 111, 3922
- Laurie V. 1956, *J. Chem. Phys.*, 24, 635
- Lee, K.L.L., Changala, P.B., Loomis, R.A., et al. 2021, *ApJ*, 910, L2
- Léger, A., Puget, J.L. 1984, *A&A*, 137, L5
- Li, Y.S., Jalilian, M.R., Durig, J.R. 1979, *J. Mol. Struct.*, 51, 171
- Loison, J.-C. & Bergeat, A. 2009, *PCCP*, 11, 655
- McGuire, B.A., Burkhardt, A.M., Kalenskii, S., et al. 2018, *Science*, 359, 202
- McGuire, B.A., Loomis, R.A., Burkhardt, A.M., et al. 2021, *Science*, 371, 1265
- Mangum, J.G. & Wooten, A. 1990, *A&A*, 239, 319
- Marcelino, N., Cernicharo, J., & Agúndez, M. 2007, *ApJ*, 665, L127
- Marcelino, N., Agúndez, M., Tercero, B., et al. 2020, *A&A*, 643, L6
- Marcelino, N., Tercero, B., Agúndez, M., & Cernicharo, J. 2021, *A&A*, 646, L9
- Martínez, L., Santoro, G., Merino, P., et al. 2020, *Nature Astron.*, 4, 97
- Matthews, H.E. & Irvine, W.M. 1985, *ApJ*, 298, L61
- Matthews, H.E., Madden, S.C., Avery, L.W. & Irvine, W.M. 1986, *ApJ*, 307, L69
- McCarthy, M.C., Travers, M.J., Kovacs, A. et al. 1997, *Science*, 275, 518
- McCarthy, M.C., Grabow, J.-U., Travers, M.J. et al. 1999, *ApJ*, 513, 305
- McCarthy, M.C., Lee, K.L.K., Loomis, R.A., et al. 2021, *Nature Astron.*, 5, 176
- Mebel, A. M., Landera, A., & Kaiser, R. I. 2017, *J. Phys. Chem. A*, 121, 901
- Miller, J.A., Klippenstein, S.J., & Robertson, S. H. 2000, *J. Phys. Chem. A*, 104, 7525
- Müller, H.S.P., Schlöder, F., Stutzki, J., Winnewisser, G. 2005, *J. Mol. Struct.*, 742, 215
- Pickett, H.M., Poynter, R. L., Cohen, E. A., et al. 1998, *J. Quant. Spectrosc. Radiat. Transfer*, 60, 883
- Pillari, P., Joblin, C., Boulanger, F. & Onaka, T. 2015, *A&A*, 577, A16
- Pratap, P., Dickens, J. E., Snell, R. L., et al. 1997, *ApJ*, 486, 862
- Ribeiro, J.M. & Mebel, A.M. 2016, *J. Phys. Chem. A*, 120, 1800
- Saeyns, M., Reyniers, M.-F., Marin, G. B., et al. 2003, *J. Phys. Chem. A*, 107, 9147
- Scharpen, L.H. & Laurie, V. 1965, *J. Chem. Phys.*, 43, 2765
- Seburg, R.A., McMahon, R.J., Stanton, J.F., & Gauss, 119, 10838J. 1997, *J. Am. Chem. Soc.*, 119, 10838
- Sims, I. R., Queffelec, J.-L., Travers, D., et al. 1993, *Chem. Phys. Lett.*, 211, 461
- Tercero, F., López-Pérez, J. A., Gallego, et al. 2021, *A&A*, 645, A37
- Travers, M.J., McCarthy, M.C., Gottlieb, C.A., & Thaddeus, P. 1997, *ApJ*, 483, L135
- Turner, B.E., Herbst, E. & Terzieva, R. 2000, *ApJS*, 126, 427
- Yamamoto, S., Saito, S., Ohishi, M., et al. 1987, *ApJ*, 322, L55
- Vakhtin, A.B., Heard, D.E., Smith, I.W.M., & Leone, S.R. 2001, *Chem. Phys. Lett.*, 344, 317
- Vereecken, L. & Peeters, J. 2003, *PCCP*, 5, 2807
- Woods, P.M., Millar, T. J., & Zijlstra, A.A. 2002, *ApJ*, 574, L167

Appendix A: Line parameters of *c*-C₃HCCH, *c*-C₅H₆, and *c*-C₉H₈

Line parameters for the different molecules studied in this work were obtained by fitting a Gaussian line profile to the observed data. A window of $\pm 15 \text{ km s}^{-1}$ around the v_{LSR} of the source has been considered for each transition. The derived line parameters for the three molecular species discovered in this work are given in Table A.1.

Table A.1. Observed line parameters for c-C₃HCCH in TMC-1

J_{K_a, K_c}	ν_{obs}^a (MHz)	$\int T_A^* dv^b$ (mK km s ⁻¹)	Δv^c (km s ⁻¹)	T_A^{*d} (mK)	
<i>c</i> -C ₃ HCCH					
1 _{1,0} – 1 _{0,1}	31525.012±0.03	1.30±0.23	1.35±0.28	0.90±0.20	
2 _{1,1} – 2 _{0,2}	31838.475±0.03	1.98±0.34	1.34±0.20	1.38±0.24	
5 _{1,5} – 4 _{1,4}	31904.045±0.03	0.53±0.18	0.76±0.35	0.65±0.24	A
3 _{1,2} – 3 _{0,3}	32312.929±0.03	0.87±0.16	0.87±0.17	0.93±0.20	A
9 _{0,9} – 8 _{1,8}	32429.470±0.03	0.88±0.20	1.13±0.28	0.73±0.21	
5 _{0,5} – 4 _{0,4}	32646.191±0.03	1.34±0.19	1.32±0.24	0.95±0.18	
4 _{1,3} – 4 _{0,4}	32953.663±0.03	1.07±0.22	1.16±0.33	0.87±0.22	
5 _{1,4} – 4 _{1,3}	33460.002±0.03	0.70±0.20	0.40±0.23	1.35±0.22	B
5 _{1,4} – 5 _{0,5}	33767.455±0.03	1.24±0.23	1.18±0.24	0.88±0.21	
6 _{1,5} – 6 _{0,6}	34762.885±0.03	1.09±0.25	1.37±0.38	0.75±0.21	
7 _{1,6} – 7 _{0,7}	35950.042±0.02				C
8 _{1,7} – 8 _{0,8}	37340.311±0.02				D
1 _{1,1} – 0 _{0,0}	37752.281±0.01				E
6 _{1,6} – 5 _{1,5}	38278.543±0.01				C
9 _{1,8} – 9 _{0,9}	38946.462±0.03				E
6 _{0,6} – 5 _{0,5}	39149.938±0.03	0.75±0.15	0.87±0.16	0.80±0.21	
10 _{0,10} – 9 _{1,9}	40056.165±0.03	1.06±0.18	0.81±0.20	1.23±0.21	
2 _{1,2} – 1 _{0,1}	43979.464±0.03	0.98±0.18	0.96±0.19	0.95±0.26	
<i>c</i> -C ₅ H ₆ ^f					
3 _{1,2} – 2 _{2,1}	37454.017±0.02	1.18±0.22	0.79±0.16	1.40±0.30	
3 _{2,2} – 2 _{1,1}	38092.525±0.02	0.85±0.17	0.68±0.15	1.17±0.24	
4 _{0,4} – 3 _{1,3}	38224.588 ^e				F
4 _{1,4} – 3 _{0,3}	38224.787±0.02	0.75±0.14	0.68±0.15	1.03±0.20	
4 _{1,3} – 3 _{2,2}	46314.423 ^e			≤1.5	
4 _{2,3} – 3 _{1,2}	46352.738±0.02	1.37±0.26	0.56±0.12	2.33±0.47	
3 _{3,1} – 2 _{2,0}	46499.116±0.02	0.91±0.18	0.48±0.09	1.78±0.36	
5 _{0,5} – 4 _{1,4}	46767.415±0.02	3.49±0.23	0.62±0.05	5.33±0.39	G
<i>c</i> -C ₉ H ₈ ^f					
11 _{4,7} – 10 _{4,6}	31364.868±0.02	0.47±0.20	1.12±0.39	0.40±0.20	
12 _{3,10} – 11 _{3,9}	32083.322±0.01	0.80±0.18	1.11±0.32	0.68±0.18	
11 _{3,8} – 10 _{3,7}	32171.624±0.01	0.83±0.28	0.89±0.33	0.88±0.20	
13 _{2,12} – 12 _{2,11}	32481.036±0.01	0.74±0.16	0.83±0.18	0.84±0.21	
14 _{0,14} – 13 _{1,13}	32526.303±0.01	0.94±0.20	1.01±0.24	0.87±0.18	
14 _{1,14} – 13 _{1,13}	32527.242±0.01	0.78±0.21	1.05±0.33	0.70±0.18	
14 _{0,14} – 13 _{0,13}	32528.322±0.01	1.14±0.21	1.65±0.15	0.65±0.18	
14 _{1,14} – 13 _{0,13}	32529.269±0.01	0.61±0.19	0.60±0.24	0.97±0.20	
13 _{1,12} – 12 _{1,11}	32555.319±0.03	1.15±0.26	1.87±0.45	0.57±0.20	A
12 _{2,10} – 11 _{2,9}	33087.091±0.02	0.21±0.11	0.48±0.20	0.40±0.16	
12 _{6,7} – 11 _{6,6}	33104.538±0.01			≤0.48	
12 _{4,9} – 11 _{4,8}	33105.876±0.02	0.30±0.16	0.40±0.20	0.45±0.16	
12 _{6,6} – 11 _{6,5}	33124.468±0.02	0.56±0.17	0.84±0.19	0.70±0.19	A
12 _{5,8} – 11 _{5,7}	33262.106±0.01	0.91±0.18	0.81±0.20	1.05±0.22	
12 _{5,7} – 11 _{5,6}	33524.184±0.02	0.26±0.10	0.34±0.20	0.72±0.18	
13 _{3,11} – 12 _{3,10}	34484.248±0.01	0.72±0.16	0.96±0.26	0.70±0.18	
12 _{4,8} – 11 _{4,7}	34608.352±0.01	0.88±0.16	1.11±0.22	0.75±0.18	
14 _{2,13} – 13 _{2,12}	34736.637±0.01	0.60±0.19	1.02±0.36	0.55±0.21	
15 _{0,15} – 14 _{1,14}	34771.228±0.02			≤0.45	
15 _{1,15} – 14 _{1,14}	34771.684±0.02	0.30±0.08	0.54±0.17	0.53±0.15	
15 _{0,15} – 14 _{0,14}	34772.190±0.02	0.49±0.32	0.94±0.33	0.49±0.15	A
15 _{1,15} – 14 _{0,14}	34772.612±0.02			≤0.45	
14 _{1,13} – 13 _{1,12}	34776.320±0.02	0.40±0.08	0.33±0.15	1.13±0.17	
12 _{3,9} – 11 _{3,8}	35011.580±0.01	0.57±0.13	0.63±0.15	0.85±0.19	
13 _{2,11} – 12 _{2,10}	35211.250±0.01	0.43±0.08	0.49±0.22	0.82±0.17	
13 _{4,10} – 12 _{4,9}	35766.651±0.02	0.68±0.17	1.12±0.26	0.57±0.19	
13 _{6,8} – 12 _{6,7}	35959.203±0.01			≤0.60	
13 _{6,7} – 12 _{6,6}	36008.349±0.02	0.64±0.15	1.00±0.34	0.60±0.20	A
13 _{5,9} – 12 _{5,8}	36101.117±0.02	0.64±0.17	1.10±0.40	0.47±0.16	
13 _{5,8} – 12 _{5,7}	36605.949±0.01	0.71±0.15	0.71±0.15	0.94±0.21	

Table A.1. continued.

J_{K_a,K_c}	ν_{obs}^a (MHz)	$\int T_A^* dv^b$ (mK km s ⁻¹)	$\Delta\nu^c$ (km s ⁻¹)	T_A^{*d} (mK)	
14 _{3,12} – 13 _{3,11}	36835.520±0.01	0.80±0.16	1.02±0.25	0.74±0.18	
15 _{2,14} – 14 _{2,13}	36986.145±0.02	0.32±0.11	0.45±0.16	0.59±0.19	
15 _{1,14} – 14 _{1,13}	37006.756±0.01	0.60±0.14	0.65±0.16	0.87±0.19	
16 _{1,16} – 15 _{1,15}	37016.001±0.02	0.39±0.15	0.77±0.27	0.47±0.20	
16 _{0,16} – 15 _{0,15}	37016.269±0.02	0.68±0.21	1.05±0.35	0.57±0.20	A
14 _{2,12} – 13 _{2,11}	37318.440±0.01	0.30±0.12	0.60±0.20	0.47±0.20	
13 _{3,10} – 12 _{3,9}	37665.778±0.01	0.84±0.16	0.78±0.17	1.01±0.21	
13 _{4,9} – 12 _{4,8}	37842.548±0.01	0.41±0.16	0.64±0.21	0.70±0.19	
14 _{4,11} – 13 _{4,10}	38361.360±0.01				C
14 _{6,9} – 13 _{6,8}	38829.224±0.01	0.87±0.17	0.83±0.16	1.00±0.23	
14 _{5,10} – 13 _{5,9}	38918.551±0.01			≤0.69	
14 _{6,8} – 13 _{6,7}	38939.641±0.02			≤0.69	
15 _{3,13} – 14 _{3,12}	39147.950±0.02	0.38±0.13	0.48±0.20	0.75±0.23	
16 _{2,15} – 15 _{2,14}	39232.293±0.02	1.02±0.27	0.68±0.19	1.46±0.24	
16 _{1,15} – 15 _{1,14}	39242.748±0.02			≤1.6	
17 _{1,17} – 16 _{1,16}	39260.308±0.02	0.71±0.23	0.54±0.18	1.21±0.40	
17 _{0,17} – 16 _{0,16}	39260.513±0.02	1.04±0.26	0.61±0.15	1.61±0.40	
15 _{2,13} – 14 _{2,12}	39447.608±0.03	0.54±0.18	0.82±0.29	0.62±0.22	
14 _{5,9} – 13 _{5,8}	39799.463±0.03	0.51±0.18	1.10±0.33	0.43±0.20	
14 _{3,11} – 13 _{3,10}	40118.461±0.02			≤0.65	
15 _{4,12} – 14 _{4,11}	40886.724±0.03	0.58±0.20	0.95±0.35	0.57±0.26	
14 _{4,10} – 13 _{4,9}	40983.754±0.03	0.37±0.17	0.60±0.29	0.58±0.24	
16 _{3,14} – 15 _{3,13}	41432.310±0.03			≤0.90	
17 _{2,16} – 16 _{2,15}	41476.748±0.03				B
17 _{1,16} – 16 _{1,15}	41482.002±0.03			≤0.90	
18 _{1,18} – 17 _{1,17}	41504.704±0.01	0.95±0.20	0.74±0.18	1.21±0.29	H
18 _{0,18} – 17 _{0,17}	41504.704±0.01				H
16 _{2,14} – 15 _{2,13}	41608.793±0.02	0.63±0.27	0.49±0.17	1.20±0.33	
15 _{5,11} – 14 _{5,10}	41698.205±0.02			≤0.90	
19 _{1,19} – 18 _{1,18}	43748.996±0.02	1.00±0.30	0.92±0.38	1.09±0.35	H
19 _{0,19} – 18 _{0,18}	43748.996±0.02				H
20 _{1,20} – 19 _{1,19}	45993.359±0.02	1.24±0.31	0.64±0.23	1.83±0.42	H
20 _{0,20} – 19 _{0,19}	45993.369±0.02				H

Notes.^(a) Observed frequency assuming a ν_{LSR} of 5.83 km s⁻¹.^(b) Integrated line intensity in mK km s⁻¹.^(c) Linewidth at half intensity derived by fitting a Gaussian function to the observed line profile (in km s⁻¹).^(d) Antenna temperature in milli Kelvin.^(e) Predicted frequency.^(f) Measured frequencies assume a ν_{LSR} of 5.83 km s⁻¹. The difference between observed and predicted frequencies are ±15 kHz.^(A) Partially blended with another feature. Fit still possible providing reasonable results.^(B) Blended with another feature. Fit uncertain.^(C) Fully blended with a negative feature produced in the frequency switching folding. Fit unreliable. Frequency corresponds to the predicted value from the rotational constants of Table 1.^(D) Fully blended with a line from HCCCH₂CN. Frequency corresponds to the predicted value from the rotational constants of Table C.1.^(E) A narrow line is clearly visible but it is affected by a negative feature. Frequency corresponds to the predicted value from the rotational constants of Table 1.^(F) Fully blended with a line from *c*-C₃HD. Frequency corresponds to the predicted value.^(G) The 5_{1,5} – 4_{0,4} line, which belongs to the para species, is fully blended with the 5_{0,5} – 4_{1,4} transition of the ortho species. Both lines have similar line strength.^(H) Unresolved doublet.

Appendix B: The isomers of $c\text{-C}_3\text{HCCH}$

The isomeric family with formula H_2C_5 is composed by five molecular species. The nonpolar pentadiynylidene (HCCCCH) and ethynyl cyclopropenylidene ($c\text{-C}_3\text{HCCH}$) are the most stable isomers, whose energy separation is very small ~ 0.043 eV. H_2CCCCC is a high energy isomer and lies 0.564 eV above the ground. Other two species are part of this isomeric family, HCC(CH)CC and $c\text{-C}_3\text{H}_2\text{CC}$, placed at 0.737 and 0.910 eV respectively, above the most stable forms, respectively (Seburg et al. 1997).

The rotational transitions in the 31-50 GHz of HCC(CH)CC, one of the C_5H_2 isomers, can be predicted with high accuracy from the laboratory data of Gottlieb et al. (1998). We obtain a 3σ upper limit to its column density of $2 \times 10^{10} \text{ cm}^{-2}$. Note that the dipole moment of this species is 4.52 D (Gottlieb et al. 1998). An even larger dipole moment has been calculated by the same authors for the isomer $c\text{-C}_3\text{H}_2\text{CC}$ (8.2 D). For this species we derive a 3σ upper limit to its column density of $9 \times 10^9 \text{ cm}^{-2}$. Finally, the cumulenic species H_2C_5 has been detected recently from our data and the results will be published elsewhere (Cabezas et al. 2021, in preparation).

An additional derivate of $c\text{-C}_3\text{H}_2$ is cyano propenylidene, $c\text{-C}_3\text{HCN}$, which has been observed in the laboratory by McCarthy et al. (1999). We searched for it in our data and derive a 3σ upper limit to its column density of $2.5 \times 10^{11} \text{ cm}^{-2}$.

Appendix C: Improved rotational constants for $c\text{-C}_3\text{HCCH}$ and $c\text{-C}_9\text{H}_8$

The frequencies we have measured in TMC-1 can be used to improve the rotational and distortion constants of $c\text{-C}_3\text{HCCH}$ and indene. We have used the fitting code FITWAT described in Cernicharo et al. (2018).

Table C.1 provides the results obtained by fitting the laboratory data of Travers et al. (1997) for $c\text{-C}_3\text{HCCH}$ alone, and those obtained from a fit to the merged laboratory plus the TMC-1 frequencies. An improvement of the uncertainty in the rotational and distortion constants is obtained. The fit to the laboratory data alone results in exactly the same constants than those obtained by Travers et al. (1997).

Table C.2 provide the same information but for indene. The 50 lines measured in TMC-1 (three of them are unresolved doublets) provide a significant improvement of the rotational and distortion constants for this species.

The merged fits are recommended to predict the frequency of the rotational transitions of both species with uncertainties between 10 and 200 kHz up to 115 GHz.

Appendix D: Column density of $c\text{-C}_3\text{H}_2$

The polar carbene ring molecule $c\text{-C}_3\text{H}_2$ is widespread in interstellar and circumstellar clouds (Matthews & Irvine 1985). For the physical conditions of TMC-1 we expect only a few lines of this molecule to be strong enough within the frequency coverage of our survey. In fact, only one ortho line, the $3_{21} - 3_{12}$ at 44104.777 MHz has an upper energy level below 20 K. This line appears in our data in absorption as shown in Fig. D.1. We have checked that the absorption is real and not produced by a negative feature created during the folding of the frequency switching data by analyzing separately the two frequency throws used during the observations. This line was predicted to be in absorption by Avery & Green (1989) for the typical densities of cold dark clouds, but to the best of our knowledge it has not been reported

Table C.1. Rotational and distortion constants of $c\text{-C}_3\text{HCCH}$

Constant	Laboratory ^a	This work
A (MHz)	34638.7012(27)	34638.7023(26)
B (MHz)	3424.87685(43)	3424.87678(42)
C (MHz)	3113.63856(50)	3113.63900(44)
Δ_J (kHz)	0.2877(80)	0.2918(74)
Δ_{JK} (kHz)	29.53(24)	29.72(21)
Number of lines	13	26
σ (kHz)	2.1	26
J_{max}, K_{max}	7, 1	10, 1
ν_{max} (GHz)	26.130	43.979

Notes.

Values between parenthesis correspond to the uncertainties of the parameters in units of the least significant digits.

^(a) Laboratory frequencies from Travers et al. (1997).

Table C.2. Rotational and distortion constants of $c\text{-C}_9\text{H}_8$

Constant	Laboratory ^a	This work
A (MHz)	3775.048(15)	3775.0469(80)
B (MHz)	1580.8656(21)	1580.86511(79)
C (MHz)	1122.2460(18)	1122.24773(51)
Δ_J (kHz)	0.0326(38)	0.03349(97)
Δ_{JK} (kHz)	0.050(11)	0.0517(73)
Δ_K (kHz)	0.37(12)	0.329(82)
δ_J (kHz)	0.0117(12)	0.01068(51)
δ_K (kHz)	0.068(19)	0.0775(94)
Number of lines	78	128
σ (kHz)	67	54
J_{max}, K_{max}	30,13	30,13
ν_{max} (GHz)	39.3	45.99

Notes.

Values between parenthesis correspond to the uncertainties of the parameters in units of the least significant digits.

^(a) Laboratory frequencies from Li et al. (1979); Caminati (1993).

previously. The other two lines of the ortho species in our survey have upper level energies around 45 K and are not detected. Absorption from $c\text{-C}_3\text{H}_2$ in cold dark clouds has been previously reported for its para line $2_{20} - 2_{11}$ at 21.6 GHz (Matthews et al. 1986). For the para species three lines are detected in our data as shown in Fig. D.1. They are the $4_{40} - 4_{31}$ at 35.36 GHz, the $4_{31} - 4_{22}$ at 42.231 GHz, and the $2_{11} - 2_{02}$ at 46.755 GHz. The first one appears also in absorption. We have checked, as for $3_{21} - 3_{12}$ ortho transition, that the absorption is real. The other two para lines are in emission.

Collisional rates between $c\text{-C}_3\text{H}_2$ and He adapted to the low temperatures of cold dark clouds are available from Avery & Green (1989) and Khalifa et al. (2019). We performed Large Velocity Gradient (LVG) calculations for ortho and para cyclopropenylidene species by varying the density and the column density and by adopting the most recent set of collisional rates. The radius of the source is fixed to 40'' (Fossé et al. 2001) and the linewidth to 0.5 km s^{-1} . The best fit to the three observed para lines is obtained for $n(\text{H}_2) = (4.0 \pm 0.5) \times 10^4 \text{ cm}^{-2}$, and $N(p\text{-C}_3\text{H}_2) = (1.4 \pm 0.3) \times 10^{13} \text{ cm}^{-2}$. Adopting the derived density for the para species, then the ortho absorption line can be reproduced for a column density $N(o\text{-C}_3\text{H}_2) = 4.5 \times 10^{13} \text{ cm}^{-2}$. Hence, the ortho to para abundance ratio of $c\text{-C}_3\text{H}_2$ is ~ 3 , which is the expected value from the spin degeneracy of the two species. The total column density of cyclopropenylidene is $5.9 \times 10^{13} \text{ cm}^{-2}$, in very good agreement with the value derived by Fossé et al.

(2001) of $5.8 \times 10^{13} \text{ cm}^{-2}$. Nevertheless, the derived abundances rely on the accuracy of the collisional rate coefficients. The synthetic spectrum computed from these parameters is shown by the red (ortho) and blue (para) lines in Fig. D.1, and reproduces nicely the ortho and para absorption lines, and the two para emission lines. If we use the collisional rates calculated by Avery & Green (1989), a reasonable fit can be obtained reproducing the two absorption lines. In this case the derived volume density is $n(\text{H}_2) = (2.8 \pm 0.5) \times 10^4 \text{ cm}^{-3}$ and the best fit to the intensities correspond to $N(o\text{-C}_3\text{H}_2) = (2.8 \pm 0.5) \times 10^{13} \text{ cm}^{-2}$ and $N(p\text{-C}_3\text{H}_2) = (3.2 \pm 0.5) \times 10^{13} \text{ cm}^{-2}$. With these less accurate collisional rates the ortho/para ratio is ~ 1 . Moreover, deviations of up to 20% between calculated and observed intensities are observed for the best model fit. These deviations are not observed when we use the most recent calculations of Khalifa et al. (2019), which are based in a more precise determination of the potential energy surface of the $c\text{-C}_3\text{H}_2/\text{He}$ system. For both set of rates the derived total column density of $c\text{-C}_3\text{H}_2$ is practically identical, $\sim 6 \times 10^{13} \text{ cm}^{-2}$. In view of the complex system of absorption and emission lines shown by this molecular species, collisional rates using H_2 as collider are highly desirable.

Appendix E: Column density of $c\text{-C}_3\text{H}$

Cyclopropanediylidenyl, $c\text{-C}_3\text{H}$, has been detected towards several astrophysical environments including cold dark clouds, evolved stars, and translucent molecular clouds (Yamamoto et al. 1987; Mangum & Wooten 1990; Turner et al. 2000; Cernicharo et al. 2000). Several lines pertaining to the fine and hyperfine structure of the $2_{1,1} - 2_{1,2}$ rotational transitions of this species are within our line survey of TMC-1. The data for all the strongest components, and some of the weak ones, are shown in Fig. E.1. Several of the panels of this Figure show a significant number of unknown features. This is an important drawback for any stacking procedure used to detect molecules producing intensities below 1 mK for their rotational transitions. At this level of sensitivity TMC-1 cannot be considered as a line-poor source and detections have to be performed using the standard procedure of line-by-line detection.

With only one transition we have to assume a rotational temperature in order to derive a column density for the molecule. The energy of the upper level of the different fine and hyperfine components of the $2_{1,1} - 2_{1,2}$ transition is $\sim 6.5 \text{ K}$. Hence, the column density will depend slightly on the adopted value of T_r (see, e.g., the error analysis carried out by Cernicharo et al. 2021c for HC_3S^+). Assuming $T_r = 10 \text{ K}$, a source diameter of $80''$ and a linewidth of 0.6 km s^{-1} , we obtain a column density for $c\text{-C}_3\text{H}$ of $(1.2 \pm 0.2) \times 10^{12} \text{ cm}^{-2}$. This value is a factor five smaller than the one derived by Yamamoto et al. (1987), who observed the $2_{1,2} - 1_{1,1}$ transition at $\sim 91.5 \text{ GHz}$ with the Nobeyama radiotelescope. They assumed a rotational temperature of 5 K . In order to understand this large difference we have used the data gathered with the IRAM 30m telescope during the 3 mm line survey of TMC-1 (Marcelino et al. 2007). We obtain intensities for the $2_{1,2} - 1_{1,1}$ hyperfine components that are similar to those of Yamamoto et al. (1987). The 3 mm data are shown in Fig. E.2. Assuming an identical rotational temperature for the two transitions it is not possible to get a reliable fit to the observed intensities. In fact, the 3 mm lines are well explained with a column density of $(6.2 \pm 0.4) \times 10^{12} \text{ cm}^{-2}$ for $T_r = 5 \text{ K}$, a very similar value to that of Yamamoto et al. (1987). However, the rotational temperature has to be decreased to 3.7 K to explain with the same column density the observed intensities for the $2_{1,1} - 2_{1,2}$. The two transitions share the same lower level (the

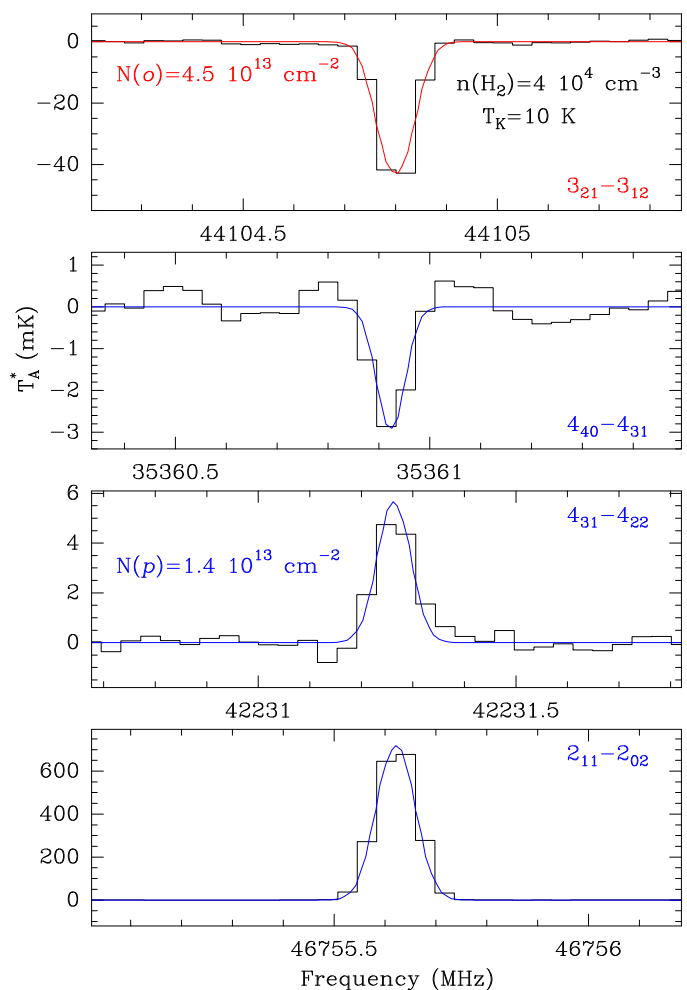


Fig. D.1. Observed transitions of $c\text{-C}_3\text{H}_2$ in TMC-1. The abscissa corresponds to the rest frequency of the lines assuming a local standard of rest velocity of the source of 5.77 km s^{-1} . The ordinate is the antenna temperature, corrected for atmospheric and telescope losses, in mK. The quantum numbers for each transition are indicated in the upper or lower right corner of the corresponding panel. The red line shows the computed synthetic spectrum for this species (see text). Blue labels indicate the multiplicative factor applied, when needed, to the model to match the intensity of the observed lines.

fundamental one), but they could have significant different excitation temperatures if the collisional rates from the ground to the two upper levels are different. Unfortunately no collisional rates for $c\text{-C}_3\text{H}$ are available in the literature.

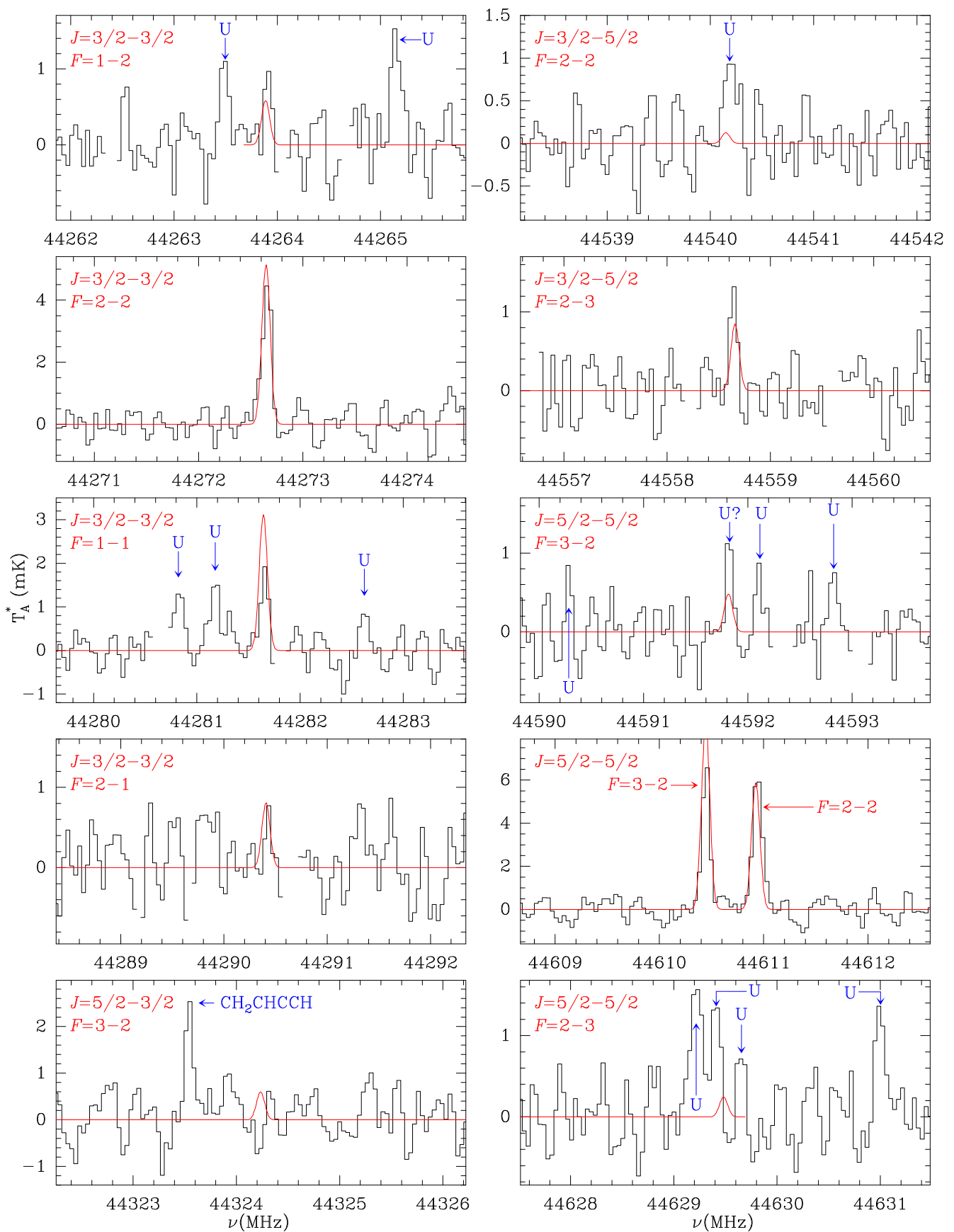


Fig. E.1. Fine and hyperfine components of the $2_{1,1} - 1_{1,1}$ transition of $c\text{-C}_3\text{H}$ in TMC-1 as observed with the Yebes 40m radiotelescope. The abscissa corresponds to the rest frequency of the lines assuming a local standard of rest velocity of the source of 5.83 km s^{-1} . The ordinate is the antenna temperature, corrected for atmospheric and telescope losses, in mK. The quantum numbers for each transition are indicated in the upper or lower right corner of the corresponding panel. The red line shows the computed synthetic spectrum for this species for a column density of $6.2 \times 10^{12} \text{ cm}^{-2}$ and $T_r = 3.7 \text{ K}$ (see text).

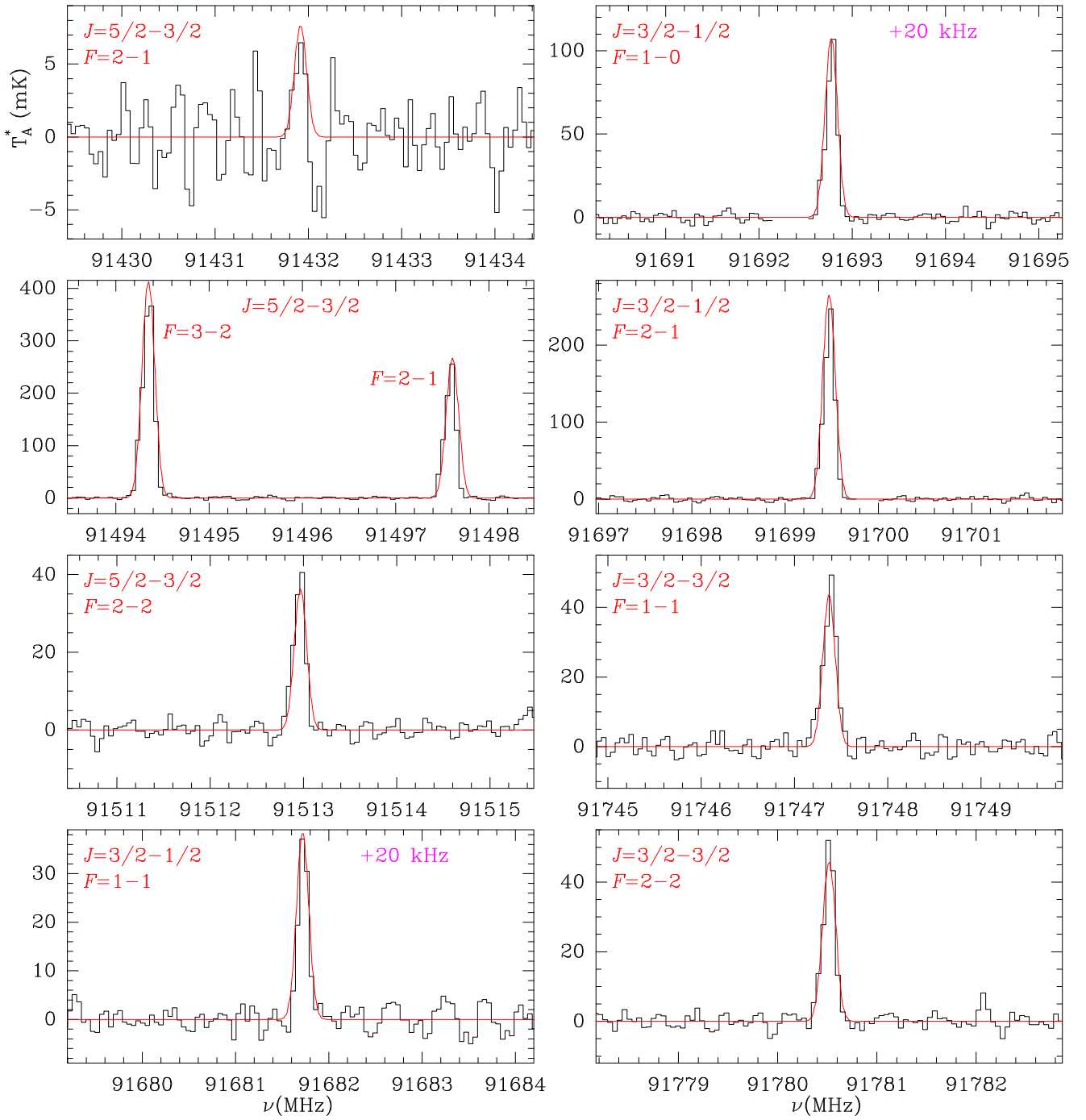


Fig. E.2. Fine and hyperfine components of the $2_{1,2} - 1_{1,1}$ transition of $c\text{-C}_3\text{H}$ in TMC-1 as observed with the IRAM 30m radiotelescope (data from Marcelino et al. 2007). The abscissa corresponds to the rest frequency of the lines assuming a local standard of rest velocity of the source of 5.83 km s^{-1} . The ordinate is the antenna temperature, corrected for atmospheric and telescope losses, in mK. The quantum numbers for each transition are indicated in the upper or lower right corner of the corresponding panel. The red line shows the computed synthetic spectrum for this species for a column density of $6.2 \times 10^{12} \text{ cm}^{-2}$ and $T_r = 5 \text{ K}$ (see text). Violet labels indicate the observed minus calculated frequencies when larger than 5 kHz.